# Benchmarking of augmented Lagrangian and Hamiltonian formulations for multibody system dynamics

**Francisco González*, Daniel Dopico*, Roland Pastorino*†, Javier Cuadrado***

*Laboratorio de Ingeniería Mecánica
University of La Coruña
Mendizábal s/n, 15403 Ferrol, Spain
[f.gonzalez, ddopico,
rpastorino, javicuad]@udc.es

† PMA division,
Department of Mechanical Engineering
KU Leuven
Celestijnenlaan 300b, 3001 Leuven, Belgium
roland.pastorino@mech.kuleuven.be

**Abstract**

Augmented Lagrangian methods represent an efficient way to carry out the forward-dynamics simulation of mechanical systems. These algorithms introduce the constraint forces in the dynamic equations of the system through the use of a set of multipliers. While most of these formalisms were obtained using the system Lagrange's equations as starting point, a number of them have been derived from Hamilton's canonical equations. Besides being efficient, they are generally considered to be very robust, which makes them especially suitable for the simulation of systems with discontinuities and impacts. In this work, we have focused on the simulation of mechanical assemblies that undergo singular configurations. First, some sources of numerical difficulties in the proximity of singular configurations were identified and discussed. Afterwards, several augmented Lagrangian and Hamiltonian formulations were compared in terms of their robustness during the forward-dynamics simulation of two benchmark problems. The effect of the formulation and numerical integrator choice and parameters on the simulation performance was also assessed.

**Keywords:** Multibody system dynamics, augmented Lagrangian methods, singular configurations

## 1 Introduction

Forward-dynamics simulation of multibody systems is a relatively new area in the field of Mechanics. The progress in computer architectures and software tools during the last decades has boosted both research and industry applications of this technique. Real-time applications such as Human- and Hardware-in-the-Loop (HiL) setups are especially demanding in terms of both efficiency and robustness. As a consequence, a considerable effort has been made within the multibody community to develop fast and reliable simulation algorithms to satisfy these requirements.

Generally speaking, multibody systems consist of a set of rigid or flexible links interconnected by joints. The consideration of the kinematic constraints introduced by the latter usually leads to the need for expressing the dynamics equations as a system of Differential Algebraic Equations (DAE's). Different approaches can be used to solve such a system, among which Lagrange's multiplier method is a widely used one [1].

If a mechanical system is described with a set of $n$ generalized coordinates $\mathbf{q}$, subjected to $m$ holonomic kinematic constraints $\mathbf{\Phi}$, the equations of motion can be expressed as

$$\mathbf{M}\ddot{\mathbf{q}} + \mathbf{c} = \mathbf{f} + \mathbf{f}_c \tag{1a}$$

$$\mathbf{\Phi}(\mathbf{q}, t) = \mathbf{0} \tag{1b}$$

where $\mathbf{M}$ is the $n \times n$ mass matrix, $\mathbf{c}$ contains the Coriolis and centrifugal forces, and $\mathbf{f}$ and $\mathbf{f}_c$ are the applied and constraint forces, respectively. Following a Lagrangian approach, the generalized constraint reactions can be expressed as $\mathbf{f}_c = -\mathbf{\Phi}_\mathbf{q}^\mathrm{T}\boldsymbol{\lambda}$, where $\mathbf{\Phi}_\mathbf{q} = \partial\mathbf{\Phi}/\partial\mathbf{q}$ is the $m \times n$ Jacobian matrix of the constraints and $\boldsymbol{\lambda}$ is a set of $m$ Lagrange multipliers.

One of the first augmented Lagrangian algorithms for multibody dynamics was introduced by Bayo et al. in [2]. The proposed method combined a penalty representation of the constraint

forces with an iterative update of the Lagrange multipliers. An extension of the method to handle nonholonomic constraints was also included in [2]. Subsequently, several related methods based on the augmented Lagrangian approach have been developed and can be found in the literature. An implementation of the algorithm in [2] aimed at real-time efficiency was published in [3]. In [4] and [5] mass-orthogonal projections were used together with the augmented-Lagrangian formulation to ensure the satisfaction of the kinematic constraints. These two papers included index-3 versions of the algorithms as well, in which the dynamic equations were combined with the numerical integrator formulas. The resulting system of DAE's was solved in an iterative fashion following a Newton-Raphson scheme, thus improving the robustness of the method. The original algorithms in [4] and [5] were designed for holonomic constraints alone; an index-3 augmented Lagrangian algorithm able to deal with nonholonomic constraints was later described in [6]. The above mentioned formalisms and other similar ones have been successfully used in the study and simulation of a wide variety of mechanical systems. Application examples include heavy machinery simulators [7], biomechanics [8], and co-simulation settings for vehicle dynamics [9].

It is also possible to obtain the dynamics equations using Hamilton's canonical equations as starting point. Following this approach, the equations of motion become a system of first order Ordinary Differential Equations (ODE's) of size $2n$, instead of a system of $n$ second order ODE's. Augmented Lagrangian algorithms based on Hamilton's canonical equations can also be found in the field of multibody dynamics, e.g. [10], [11]. It was stated in [11] that the methods based on canonical equations are more robust than their classical augmented Lagrangian counterparts and ensure a better satisfaction of the kinematic constraints. This was supported by the performance comparison of two formulations, one representative of each approach, in the dynamic simulation of mechanical systems with singular configurations. Although both algorithms were able to deal with the test problems, the Hamiltonian one did not show pathological behaviour in any of the simulations carried out by the authors. However, these formulations have received comparatively less attention in the literature since they were first presented to the multibody community. Naudet et al. [12] developed a recursive algorithm based on canonical momenta, although they did not follow an augmented Lagrangian approach. The authors affirm in [12] that a possible reason why Hamiltonian equations are rather infrequent in multibody applications is that they are computationally intensive to construct and they cannot compete with acceleration based algorithms, especially recursive ones. More recently, Malczyk et al. [13] combined the Divide and Conquer Algorithm (DCA) with Hamilton's canonical equations to obtain a parallel algorithm. Their preliminary results suggested that their Hamiltonian approach can outperform the Lagrangian one in terms of accuracy in the enforcement of kinematic constraints and conservation of the mechanical energy of the system.

In this paper, a performance study of several existing augmented Lagrangian and Hamiltonian methods for multibody dynamics is presented. Special attention was paid to their behaviour in the proximity of singular configurations. The comparison of the different algorithms was done using test examples from the IFToMM benchmark problem library [14].

## 2 Augmented Lagrangian formulations

Several formulations were selected for this study among the many available in the literature. The ones described in [2], [11], and [4] were chosen because they share a similar structure of the dynamics equations. In the following, natural coordinates [15] are assumed to be used in the modelling. This has two important consequences. First, term $\mathbf{c}$ vanishes from the dynamics equations. Second, the mass matrix $\mathbf{M}$ becomes constant, and so all its derivatives are zero.

### 2.1 Penalty formulation

Even though it is not an augmented Lagrangian one, it is convenient to briefly describe here the penalty formulation introduced in [2]. This formulation replaces the kinematic constraints $\mathbf{\Phi}$ with

penalty spring-damper-mass systems. This is achieved introducing fictitious potential and kinetic energy terms in the integral action $A$ of the mechanical system, as well as a set of dissipative forces. The constraint reactions are then replaced by forces proportional to the constraint violations at the acceleration, velocity, and configuration levels

$$\boldsymbol{\lambda} = \alpha \left( \ddot{\boldsymbol{\Phi}} + 2\xi\omega\dot{\boldsymbol{\Phi}} + \omega^2 \boldsymbol{\Phi} \right) \tag{2}$$

where $\alpha$ is the penalty factor, and $\xi$ and $\omega$ are Baumgarte's stabilization parameters [16]. Together with the velocity- and acceleration-level expression of the kinematic constraints $\boldsymbol{\Phi}$

$$\dot{\boldsymbol{\Phi}} = \boldsymbol{\Phi}_{\mathbf{q}} \dot{\mathbf{q}} + \boldsymbol{\Phi}_t = \mathbf{0} \tag{3}$$

$$\ddot{\boldsymbol{\Phi}} = \boldsymbol{\Phi}_{\mathbf{q}} \ddot{\mathbf{q}} + \dot{\boldsymbol{\Phi}}_{\mathbf{q}} \dot{\mathbf{q}} + \dot{\boldsymbol{\Phi}}_t = \mathbf{0} \tag{4}$$

where $\boldsymbol{\Phi}_t = \partial \boldsymbol{\Phi} / \partial t$, Eq. (2) allows for the transformation of the system of DAE's (1) into a system of $n$ second order ODE's

$$\left( \mathbf{M} + \boldsymbol{\Phi}_{\mathbf{q}}^{\mathrm{T}} \alpha \boldsymbol{\Phi}_{\mathbf{q}} \right) \ddot{\mathbf{q}} = \mathbf{f} - \boldsymbol{\Phi}_{\mathbf{q}}^{\mathrm{T}} \alpha \left( \dot{\boldsymbol{\Phi}}_{\mathbf{q}} \dot{\mathbf{q}} + \dot{\boldsymbol{\Phi}}_t + 2\xi\omega\dot{\boldsymbol{\Phi}} + \omega^2 \boldsymbol{\Phi} \right) \tag{5}$$

Terms $\alpha$, $\xi$, and $\omega$ are $n \times n$ matrices in the general case but for simplicity they are treated as scalars in this document.

### 2.2 Index-1 and index-3 augmented Lagrangian formulations

The penalty formulation in Eq. (5) has the disadvantage of being very sensitive to the value of the penalty factor $\alpha$ in terms of convergence. Additionally, a certain violation of constraints is required to develop the necessary reaction forces $\mathbf{f}_c$, so a complete fulfilment of the constraints can never be achieved. The augmented Lagrangian formulations proposed in [2] and [4] intended to overcome these limitations. The Lagrange multiplier method was applied to the solution of Eq. (5) to obtain the index-1 iterative algorithm

$$\begin{aligned} \left( \mathbf{M} + \boldsymbol{\Phi}_{\mathbf{q}}^{\mathrm{T}} \alpha \boldsymbol{\Phi}_{\mathbf{q}} \right) \ddot{\mathbf{q}} + \boldsymbol{\Phi}_{\mathbf{q}}^{\mathrm{T}} \boldsymbol{\lambda}^* &= \mathbf{f} - \boldsymbol{\Phi}_{\mathbf{q}}^{\mathrm{T}} \alpha \left( \dot{\boldsymbol{\Phi}}_{\mathbf{q}} \dot{\mathbf{q}} + \dot{\boldsymbol{\Phi}}_t + 2\xi\omega\dot{\boldsymbol{\Phi}} + \omega^2 \boldsymbol{\Phi} \right) \\ \boldsymbol{\lambda}_{i+1}^* &= \boldsymbol{\lambda}_i^* + \alpha \left( \ddot{\boldsymbol{\Phi}} + 2\xi\omega\dot{\boldsymbol{\Phi}} + \omega^2 \boldsymbol{\Phi} \right) \end{aligned} \tag{6}$$

where $\boldsymbol{\lambda}^*$ are the $m$ modified Lagrange multipliers and subscript $i$ stands for the iteration number. If the multipliers are updated only once, then this formulation is equivalent to the penalty one in Eq. (5). Position-, velocity-, and acceleration-level mass-orthogonal projections were also used in [4] to ensure an accurate satisfaction of the kinematic constraints.

In [4] and [5] the augmented Lagrangian algorithm in Eqs. (6) was combined with the Newmark numerical integration formulas [17]

$$\begin{aligned} \dot{\mathbf{q}}_{k+1} &= \frac{\gamma}{\beta h} \mathbf{q}_{k+1} - \widehat{\dot{\mathbf{q}}}_k \,; \qquad \widehat{\dot{\mathbf{q}}}_k = \frac{\gamma}{\beta h} \mathbf{q}_k + \left( \frac{\gamma}{\beta} - 1 \right) \dot{\mathbf{q}}_k + h \left( \frac{\gamma}{2\beta} - 1 \right) \\ \ddot{\mathbf{q}}_{k+1} &= \frac{1}{\beta h^2} \mathbf{q}_{k+1} - \widehat{\ddot{\mathbf{q}}}_k \,; \qquad \widehat{\ddot{\mathbf{q}}}_k = \frac{1}{\beta h^2} \mathbf{q}_k + \frac{1}{\beta h} \dot{\mathbf{q}}_k + \left( \frac{1}{2\beta} - 1 \right) \ddot{\mathbf{q}}_k \end{aligned} \tag{7}$$

where $h$ is the integration step-size, $\beta$ and $\gamma$ are scalar parameters of the integrator formulas, and subscript $k$ denotes the time-step, to obtain an index-3 algorithm with the system generalized coordinates $\mathbf{q}$ as primary integration variables. Establishing the dynamic equilibrium at time-step $k+1$ yields

$$\mathbf{M}\mathbf{q}_{k+1} + \beta h^2 \boldsymbol{\Phi}_{\mathbf{q}_{k+1}}^{\mathrm{T}} \left( \boldsymbol{\lambda}_{k+1}^* + \alpha \boldsymbol{\Phi}_{k+1} \right) - \beta h^2 \mathbf{f}_{k+1} - \beta h^2 \mathbf{M} \widehat{\ddot{\mathbf{q}}}_k = \mathbf{g}(\mathbf{q}, \dot{\mathbf{q}}) = \mathbf{0} \tag{8}$$

where the assumption that the velocity and acceleration projections remove the constraint violations at those levels has been used. The system of nonlinear equations in Eq. (8) is then solved by means of a Newton-Raphson iterative approach

$$\left[ \frac{d\mathbf{g}(\mathbf{q}, \dot{\mathbf{q}})}{d\mathbf{q}} \right]_i \Delta \mathbf{q}_{i+1} = -\mathbf{g}(\mathbf{q}, \dot{\mathbf{q}})_i \tag{9}$$

The leading matrix in Eq. (9) can be approximated as [5]

$$\left[\frac{d\mathbf{g}\left(\mathbf{q},\dot{\mathbf{q}}\right)}{d\mathbf{q}}\right] \cong \mathbf{M} + \gamma h\mathbf{C} + \beta h^2\left(\mathbf{\Phi}_\mathbf{q}^\mathrm{T}\alpha\mathbf{\Phi}_\mathbf{q} + \mathbf{K}\right) \tag{10}$$

where $\mathbf{C} = -\partial\mathbf{f}/\partial\dot{\mathbf{q}}$ and $\mathbf{K} = -\partial\mathbf{f}/\partial\mathbf{q}$. The Lagrange multipliers can be updated during the iterative process in Eq. (9) as

$$\boldsymbol{\lambda}_{i+1}^{*} = \boldsymbol{\lambda}_i^{*} + \alpha\mathbf{\Phi}_i \tag{11}$$

The index-3 augmented Lagrangian formulation (ALi3) described by Eqs. (8)–(11) with velocity and acceleration projections features excellent robustness and efficiency properties and it has been successfully used in real-time simulation of medium-size and large multibody systems [7], [9].

### 2.3 Formulation based on Hamilton's canonical equations

Formulations based on Hamilton's canonical equations constitute an alternative to the classical, acceleration-based augmented Lagrangian algorithms. They introduce the conjugate or canonical momenta $\mathbf{p} = \partial L/\partial\dot{\mathbf{q}}$, where $L$ is the system Lagrangian, as system variables besides the generalized coordinates $\mathbf{q}$ [1] . With the definition of the Hamiltonian $H = \mathbf{p}^\mathrm{T}\dot{\mathbf{q}} - L$ the canonical equations for a constrained system can be written as [11]

$$\dot{\mathbf{q}} = \frac{\partial H}{\partial\mathbf{p}}; \qquad -\dot{\mathbf{p}} = \frac{\partial H}{\partial\mathbf{q}} - \mathbf{f}_{nc} + \mathbf{\Phi}_\mathbf{q}^\mathrm{T}\boldsymbol{\lambda} \tag{12}$$

where $\mathbf{f}_{nc}$ are the non-conservative forces applied to the system. Following a procedure similar to the one described in [2], an augmented Lagrangian algorithm can be developed from Eqs. (12). Again, a fictitious potential energy term and dissipation forces are introduced in the Lagrangian and a penalty approach is followed to obtain [11]

$$\left(\mathbf{M} + \mathbf{\Phi}_\mathbf{q}^\mathrm{T}\alpha\mathbf{\Phi}_\mathbf{q}\right)\dot{\mathbf{q}} = \mathbf{p} - \mathbf{\Phi}_\mathbf{q}^\mathrm{T}\alpha\left(\mathbf{\Phi}_t + 2\xi\,\omega\mathbf{\Phi} + \omega^2\int_{t_0}^{t}\mathbf{\Phi}dt\right) - \mathbf{\Phi}_\mathbf{q}^\mathrm{T}\boldsymbol{\sigma} \tag{13}$$

where $t_0$ is the starting time of the motion and $\boldsymbol{\sigma}$ are the formulation multipliers, which verify $\dot{\boldsymbol{\sigma}} = \boldsymbol{\lambda}$. The time derivatives of the canonical momenta can be explicitly obtained from equation

$$\dot{\mathbf{p}} = \mathbf{f} + \dot{\mathbf{\Phi}}_\mathbf{q}^\mathrm{T}\alpha\left(\dot{\mathbf{\Phi}} + 2\xi\,\omega\mathbf{\Phi} + \omega^2\int_{t_0}^{t}\mathbf{\Phi}dt\right) + \dot{\mathbf{\Phi}}_\mathbf{q}^\mathrm{T}\boldsymbol{\sigma} \tag{14}$$

and the multipliers $\boldsymbol{\sigma}$ are iteratively updated following

$$\boldsymbol{\sigma}_{i+1} = \boldsymbol{\sigma}_i + \alpha\left(\dot{\mathbf{\Phi}} + 2\xi\,\omega\mathbf{\Phi} + \omega^2\int_{t_0}^{t}\mathbf{\Phi}dt\right) \tag{15}$$

The algorithm in Eqs. (13)–(15) can also be used in a penalty fashion if the number of updates of the multipliers in each evaluation of $\dot{\mathbf{q}}$ is set to just one.

## 3 Rank deficient Jacobian matrices and singular configurations

The application of the Lagrangian approach to the dynamics equations (1), together with the differentiation of the kinematic constraints (1b) with respect to time, results in a system of linear equations that can be written as follows

$$\begin{bmatrix} \mathbf{M} & \mathbf{\Phi}_\mathbf{q}^\mathrm{T} \\ \mathbf{\Phi}_\mathbf{q} & \mathbf{0} \end{bmatrix}\begin{bmatrix} \ddot{\mathbf{q}} \\ \boldsymbol{\lambda} \end{bmatrix} = \begin{bmatrix} \mathbf{f} \\ -\dot{\mathbf{\Phi}}_\mathbf{q}\dot{\mathbf{q}} - \dot{\mathbf{\Phi}}_t \end{bmatrix} \tag{16}$$

If the Jacobian matrix $\mathbf{\Phi}_\mathbf{q}$ is rank deficient, the leading matrix of system (16) becomes singular. This means that an infinite set of values of the Lagrange multipliers $\boldsymbol{\lambda}$ are valid solutions of the

system and some additional assumptions must be made to choose one solution among all the possible ones [18]. Rank deficient Jacobian matrices can be the consequence of the presence of redundant kinematic constraints. In this case, the Jacobian matrix is usually rank deficient during the whole motion of the system. Another possibility is the existence of singular configurations in the workspace. When the system reaches one of these singularities, the number of degrees of freedom (DoF) suddenly increases and the Jacobian matrix undergoes a loss of rank.

All the algorithms presented in Section 2 are able to deal with rank deficient Jacobian matrices. The leading matrices in Eqs. (5), (6), (10), and (13) are all symmetric and positive-definite, provided that an appropriate penalty factor $\alpha$ has been selected. The use of the penalty technique is equivalent to assuming a certain stiffness distribution within the system and this reduces the number of valid solutions for $\boldsymbol{\lambda}$ to only one [19]. However, they may still experience numerical difficulties in the proximity of singular configurations.

### 3.1 Benchmark examples

Several multibody systems involving redundant constraints and singular configurations can be found in the IFToMM library of benchmark problems [14]. Among these, we have selected three for the comparison of the dynamic formulations in Section 2. The first one is a six-link rectangular Bricard mechanism (Fig. 1). This is a redundantly constrained, one-DoF mechanical system frequently used as benchmark problem (e.g. [20]). The set of kinematic constraints which are linearly dependent cannot be a priori identified, as it changes during motion. Therefore, redundant equations cannot be simply eliminated from the constraint set $\boldsymbol{\Phi}$, and the Jacobian matrix $\boldsymbol{\Phi}_{\mathbf{q}}$ is permanently rank deficient. However, the system does not reach any singular configuration during its entire range of motion.

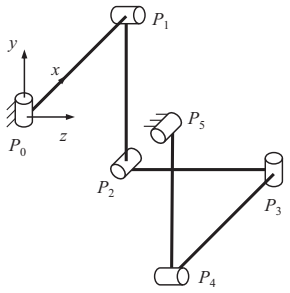


Figure 1: A six-link rectangular Bricard mechanism, a redundantly constrained multibody system without singular configurations.

Two planar linkages were chosen as examples of systems that undergo singular configurations: a slider-crank mechanism and a double four-bar linkage (Fig. 2). These were already used in [11] to discuss the performance of augmented Lagrangian formulations in the simulation of systems with singular configurations. Both are made up of rods of length $l = 1$ m with a uniformly distributed mass $m_b = 1$ kg and a square cross section of width $r = 0.1$ m, connected by revolute joints. Gravity ($g = 9.81$ m/s$^2$) acts in the negative direction of the $y$ axis in the three examples.

The forward-dynamics simulation of the motion of the Bricard mechanism can be used to show that the augmented Lagrangian formulations described in Section 2 are able to successfully deal with rank deficient Jacobian matrices derived from the presence of redundant constraints. Conversely, numerical difficulties were observed during the simulation of the systems in Fig. 2 when they were near a singular configuration.

### 3.2 Behaviour of the formulations in the neighbourhood of a singular configuration

The slider-crank mechanism in Fig. 2a is in a singular configuration when its two rods are aligned on the global $y$ axis. The linkage has one DoF during the rest of its motion, but at this configu-

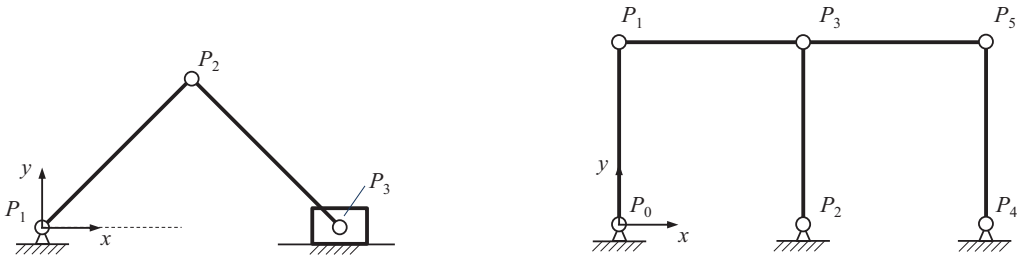


Figure 2: Benchmark problems with singular configurations: (a) slider-crank mechanism; (b) double four-bar linkage.

ration a new degree of freedom instantaneously appears. The singular configuration is in fact a bifurcation point, after which the system can continue its slider-crank motion or start to behave as a simple pendulum with point $P_3$ stopped at the global origin of coordinates. Both motions are actually possible when the linkage is exactly in the singular configuration and momentarily becomes a two-DoF system. The singular configuration for the four-bar linkage (Fig. 2b) happens when all the links are aligned on the global $x$ axis; again, we have a bifurcation point at which two alternative motions are simultaneously feasible.

### 3.2.1 Change in the subspace of admissible motion in singular configurations

It can be useful to decompose the system velocities into its components contained in the subspaces of admissible and constrained motion [21] to highlight the role of singular configurations as bifurcation points. Given a mechanical system described with a set of $n$ generalized velocities $\dot{\mathbf{q}}$, the $m$ kinematic constraints at the velocity level (3) can be used to define the subspace of constrained motion (SCM). The dimension of the SCM is the rank of the Jacobian matrix $\mathbf{\Phi_q}$, so this subspace will be $m$-dimensional if the kinematic constraints are linearly independent. The subspace of admissible motion (SAM) complements the SCM. The system velocities can be then decomposed into two components as $\dot{\mathbf{q}} = \dot{\mathbf{q}}_a + \dot{\mathbf{q}}_c$ where $\dot{\mathbf{q}}_a$ is the set of generalized velocities admissible with the velocity-level constraints in Eq. (3); $\dot{\mathbf{q}}_c$ is the velocity set which is not admissible with the constraints, i.e. constraint violations.

The slider-crank example can be modelled with three planar natural coordinates: the $x$ and $y$ coordinates of point $P_2$, $x_2$ and $y_2$, and the $x$ coordinate of point $P_3$, $x_3$. Two kinematic constraints, enforcing constant distances between the tips of the rods, are necessary to ensure the correct motion of the assembly. The corresponding equations at the velocity level are

$$\dot{\mathbf{\Phi}}^{sc} = \begin{bmatrix} 2x_2 & 2y_2 & 0 \\ 2(x_2 - x_3) & 2y_2 & 2(x_3 - x_2) \end{bmatrix} \begin{bmatrix} \dot{x}_2 \\ \dot{y}_2 \\ \dot{x}_3 \end{bmatrix} = \mathbf{\Phi}^{sc}_{\mathbf{q}} \dot{\mathbf{q}}^{sc} = \mathbf{0} \tag{17}$$

where $\dot{\mathbf{q}}^{sc}$ and $\mathbf{\Phi}^{sc}_{\mathbf{q}}$ are the generalized velocities and the Jacobian matrix of the slider crank with the selected modelling. Let us consider that at $t = 0$ link $P_1$–$P_2$ is at an angle $\phi = \phi_0 = \pi/4$ with respect to the $x$ axis, and that $\dot{x}_3 = -4$ m/s. At time $t = t_s$ the system reaches a singular configuration, in which $\phi = \pi/2$, $x_2 = x_3 = 0$, and $y_2 = l$ m. For $t < t_s$, the Jacobian matrix $\mathbf{\Phi}^{sc}_{\mathbf{q}}$ has rank two and any admissible velocity set can be expressed as

$$\dot{\mathbf{q}}^{sc}_a = \eta \begin{bmatrix} 1 \\ -x_2/y_2 \\ x_3/(x_3 - x_2) \end{bmatrix} \tag{18}$$

where $\eta$ is a scalar. At $t = t_s$, the system is in a singular configuration, and the Jacobian matrix becomes

$$\mathbf{\Phi}^{sc}_{\mathbf{q}}\big|_{t_s} = \begin{bmatrix} 0 & 2l & 0 \\ 0 & 2l & 0 \end{bmatrix} \tag{19}$$

which is a rank-1 matrix. The SCM for this instant is a one-dimensional subspace. Consequently, the SAM has dimension two. Among the several alternatives to parametrize this subspace a possible one is

$$\dot{\mathbf{q}}_a^{sc}|_{t_s} = \eta_1 \begin{bmatrix} 1 \\ 0 \\ 2 \end{bmatrix} + \eta_2 \begin{bmatrix} 1 \\ 0 \\ 0 \end{bmatrix} = \eta_1 \dot{\mathbf{q}}_{a1}^{sc} + \eta_2 \dot{\mathbf{q}}_{a2}^{sc} \tag{20}$$

where $\eta_1$ and $\eta_2$ are scalar parameters. Vector $\dot{\mathbf{q}}_{a1}^{sc}$ corresponds to the slider-crank motion of the mechanism, while $\dot{\mathbf{q}}_{a2}^{sc}$ represents a single pendulum motion with point $P_3$ fixed at the origin. The condition $x_2 = x_3$ makes both branches simultaneously possible, so the velocity vector $\dot{\mathbf{q}}$ of the system can have components along both $\dot{\mathbf{q}}_{a1}^{sc}$ and $\dot{\mathbf{q}}_{a2}^{sc}$. However, when the system leaves the singular configuration at $t > t_s$ it reverts to a one-dimensional SAM, which will be either the slider-crank one compatible with $\dot{\mathbf{q}}_{a1}^{sc}$ or the simple pendulum motion defined by $\dot{\mathbf{q}}_{a2}^{sc}$, depending on how the numerical integration process proceeded at $t = t_s$.

This reasoning can be generalized to any 1-DoF mechanical system. The introduction of an extra DoF at a singularity momentarily expands the set of admissible velocities, which becomes a linear combination of a velocity vector in continuity with the pre-existing system motion, $\dot{\mathbf{q}}_{a1}$, and a new one $\dot{\mathbf{q}}_{a2}$ which is also compatible with the constraints. Both components are only simultaneously admissible at the singular configuration; at this point $\dot{\mathbf{q}}_a = \eta_1 \dot{\mathbf{q}}_{a1} + \eta_2 \dot{\mathbf{q}}_{a2}$. After the singularity, one of the components will define the motion and the other one will become a violation of the velocity-level constraints. Augmented Lagrangian formulations based on penalty approaches transform the constraint violations into constraint reactions, as shown in Eq. (2). Accordingly, penalty-based formulations remove the velocity component along the no longer admissible direction by introducing an impact when the system leaves the singular configuration.

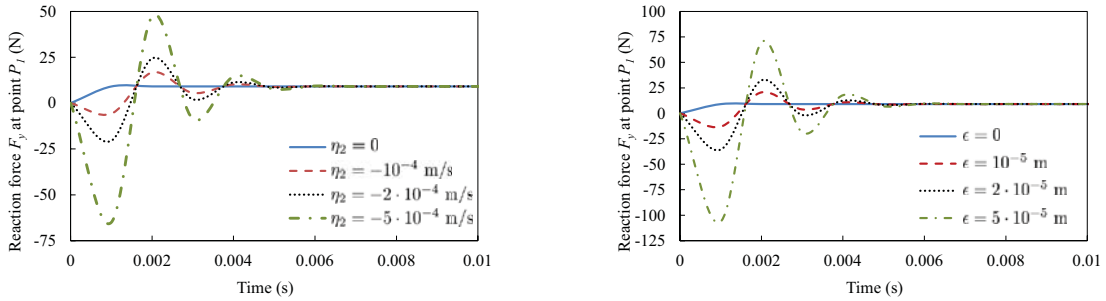


(a) (b)

Figure 3: $y$ reaction force at point $P_1$ during motion of the slider-crank mechanism, starting from a singular configuration, (a) for different initial velocities; (b) for different initial configuration-level constraint violations $\varepsilon$.

The forward-dynamics simulation of the slider-crank motion starting from the singular configuration supports the previous statements. As correctly pointed out in the literature (e.g. [11]), the simulation can be started from a singularity because the formulations in Section 2 are able to find a solution for the dynamics equations even with a rank deficient Jacobian matrix. Here, the penalty formulation in Eq. (5) was used with a penalty factor $\alpha = 10^7$, Baumgarte parameters $\omega = 10$ and $\xi = 1$, and the trapezoidal rule as integrator (a particular case of the Newmark formulas (7) with $\beta = 0.25$ and $\gamma = 0.5$), with a step-size $h = 10^{-3}$ s. First, the initial velocity was made proportional to $\dot{\mathbf{q}}_{a1}^{sc}$ by choosing $\eta_1 = -2$ m/s and $\eta_2 = 0$. Afterwards, $\eta_2$ was given different non-zero values and the simulation repeated for each of them. Fig. 3a shows that introducing a component of $\dot{\mathbf{q}}$ along $\dot{\mathbf{q}}_{a2}^{sc}$ gives rise to impact forces in the constraint reactions. Numerical experiments with the other formulations described in Section 2 showed the same behaviour. Moreover, the simulation of a 10 s motion of the four-bar linkage (Fig. 2b) confirmed that the obtained reaction force in

the $x$ direction at point $P_0$ featured the same impact forces (Fig. 4a). To obtain these results, the ALi3 formulation with velocity and acceleration projections, Eqs. (7)–(11), was used, with stringent convergence requirements to ensure that the constraint violations at the configuration and velocity levels remained close to machine precision. Similar force spikes can be observed in other publications in the literature (e.g. [22]). It should be stressed that the velocity component along $\dot{\mathbf{q}}_{a2}$ cannot be eliminated by the velocity projections at the singular configuration, because it is not a violation of the constraints at that point. As expected, these impacts are not present in the simulation of redundantly constrained mechanisms without singular configurations, as in the case of the Bricard mechanism (Fig. 1).

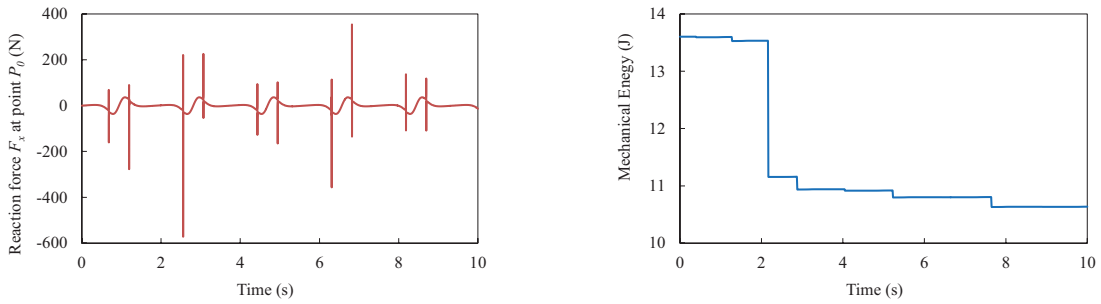


(a) (b)

Figure 4: (a) $x$ reaction force at point $P_0$ during motion of the four-bar linkage, showing impacts when the system is near a singularity; (b) mechanical energy of the slider-crank mechanism integrated with the forward Euler method ($h = 10^{-5}$ s) and the penalty formulation ($\alpha = 10^8$, $\omega = 10$, $\xi = 1$). A change of branch occurs at $t = 2.17$ s.

The impact forces above described introduce a series of undesirable effects in the simulations if the numerical integrator and the formulation parameters are not properly selected. They generate discontinuities in the mechanical energy of the system, as shown in Fig. 4b. Sometimes they can cause the mechanical system to undergo a change of branch when it leaves the singular configuration. In this case, a discontinuity in the motion takes place and the system velocities after the singularity are no longer in continuity with the pre-singularity motion compatible with $\dot{\mathbf{q}}_{a1}$, but with the secondary one defined by $\dot{\mathbf{q}}_{a2}$. In extreme cases they may bring about the failure of the simulation.

### 3.2.2 Effect of configuration-level constraint violations

The formulations in Section 2 are rather robust and they are able to handle large impact forces during the pass through singularity. Numerical simulations showed that $\eta_1$ and $\eta_2$ need be of the same order of magnitude for a change of branch to take place in most cases. The exception is the index-3 augmented Lagrangian formulation. For example, starting the simulation of the slider-crank at the singular configuration with $\eta_1 = -1$ m/s and $\eta_2 = -5 \cdot 10^{-5}$ m/s results in a pendulum motion after the singularity, with $\alpha = 10^9$ and a step-size $h = 10^{-3}$ s. Such values of $\eta_2$ are usually not reached in practice because the velocity projections keep this component small during most of the motion.

A configuration-level constraint violation, however, alters the expression of the Jacobian matrix $\mathbf{\Phi_q}$ and modifies the definition of the constrained and admissible subspaces. A modification of the generalized coordinates not compatible with the constraints, $\boldsymbol{\varepsilon}$, makes the Jacobian matrix become $\tilde{\mathbf{\Phi}}_\mathbf{q} = \mathbf{\Phi_q}(\mathbf{q} + \boldsymbol{\varepsilon})$. In general, $\tilde{\mathbf{\Phi}}_\mathbf{q}\dot{\mathbf{q}} \neq \mathbf{0}$, even though the system velocities have theoretically correct values. This means that part of the admissible generalized velocities will be treated as velocity-level constraint violations, giving rise to the impact forces described in the previous section. Fig. 3b shows the impact forces in the simulation of the slider-crank mechanism with

the penalty formulation and the same parameters of Section 3.2.1 starting from the singularity. A configuration error was introduced in the initial position by making $x_2 = -\varepsilon$ and $x_3 = \varepsilon$. The simulations showed that the effect of configuration-level constraint violations is much more critical than their velocity-level counterparts. For instance, an initial error in the order of $\varepsilon = 10^{-2}$ m is enough to trigger a branch change with $\eta_2 = 0$.

## 4 Numerical results

The existence of singular configurations is not the result of a deficient modelling or the wrong choice of simulation strategy, but a property of some mechanisms. Even though a simulation algorithm be able to deal with rank deficient Jacobian matrices, the enlargement of the SAM in the singularity points described in Section 3.2.1 remains. In fact, all the methods mentioned in Section 2 have been found to fail near singular configurations in the simulation of the slider-crank mechanism and the four-bar linkage for certain values of their $\alpha$, $\xi$, and $\omega$ parameters.

The natural motion of a mechanism would keep the continuity of the velocities during the pass through the singularities. In other words, the ideal simulation of the system motion should not introduce impact forces in the reactions at the singular configurations. Conversely, large values of these impact forces may result in discontinuities in the mechanical energy, which can lead to changes of branch or the failure of the simulation if the algorithm is unable to recover from the impact. Keeping low the violation of the kinematic constraints, especially the configuration-level ones, is a way to reduce the magnitude of the impact forces. This is in accordance with guidelines provided in the literature (e.g. [10], [11]). A simulation algorithm based on a penalty approach must therefore meet two requirements: good constraint stabilization, especially at the configuration level, and robustness to withstand impact forces. A correct adjustment of the penalty factor $\alpha$ and the stabilization parameters $\xi$ and $\omega$ is necessary to satisfy these requirements. In both the penalty and the augmented Lagrangian formulations, the constraint reactions are proportional to $\ddot{\mathbf{\Phi}}$, $\dot{\mathbf{\Phi}}$, and $\mathbf{\Phi}$ as shown in Eq. (2). Increasing the value of $\omega$ assigns more weight to the configuration-level constraint violations, which is convenient to overcome singular configurations. To achieve a similar effect in the Hamiltonian formulation in section 2.3, the term $2\xi\omega\mathbf{\Phi}$ in Eq. (15) must have a larger weight than the other terms in the equation.

Table 1: Best performances obtained with each formulation in a 10 s simulation of the slider-crank mechanism motion, for a maximum energy drift of 0.1 J. The forward Euler integration formula was used in all cases.

| Formulation | $\omega$, $\xi$ adjustment | $h$ (s) | $\alpha$ | $\omega$ | $\xi$ | elapsed time (s) |
|---|---|---|---|---|---|---|
| Penalty | manual | $2 \cdot 10^{-5}$ | $10^8$ | 25 | 1 | 1.53 |
| Penalty | automatic | $1 \cdot 10^{-5}$ | $10^6$ | $1.41 \cdot 10^5$ | 0.707 | 3.08 |
| Aug. Lagrangian | manual | $1 \cdot 10^{-5}$ | $10^7$ | 10 | 1 | 3.83 |
| Aug. Lagrangian | automatic | $1 \cdot 10^{-5}$ | $10^7$ | $1.41 \cdot 10^5$ | 0.707 | 3.85 |
| Aug. Hamiltonian | manual | $2 \cdot 10^{-3}$ | $10^9$ | 0.1 | 1000 | 0.02 |

Table 1 shows the performance of each formulation in a 10 s simulation of the slider-crank mechanism motion. The numerical experiments were carried out in an Intel Core i7-4790K at 4.00 GHz. The single-step explicit forward Euler formula was used as integrator. For the penalty and the index-1 augmented Lagrangian formulation, the $\omega$ and $\xi$ were automatically set to $\xi = 1/\sqrt{2}$ and $\omega = \sqrt{2}/h$ in a first approach [23]. These parameters were subsequently tuned to improve the simulation efficiency. This proved to be a time-consuming process with the penalty formulation, as energy conservation is noticeably affected by changes in the formulation parameters. On the other hand, the augmented Lagrangian method showed a much more consistent behaviour for a

wider range of the parameters. The parameters of the Hamiltonian formulation were manually adjusted to penalize the configuration-level constraint violations at least 200 times more than the other terms in Eq. (15). Results showed that the augmented Hamiltonian formulation described in Section 2.3 can be one or two orders of magnitude faster than the penalty or the index-1 augmented Lagrangian formulation in the studied case.

Table 2: Best performances obtained with each formulation in a 10 s simulation of the slider-crank mechanism motion, for a maximum energy drift of 0.001 J. The selected integrators were the forward Euler method (FE) and the trapezoidal rule (TR).

| Formulation | Integrator | Tolerance | $h$ (s) | $\alpha$ | $\omega$ | $\xi$ | elapsed time (s) |
|---|---|---|---|---|---|---|---|
| Aug. Hamiltonian | FE | – | $2 \cdot 10^{-5}$ | $10^9$ | 0.1 | 1000 | 2.10 |
| Penalty | TR | $10^{-7}$ | $10^{-4}$ | $10^7$ | 1000 | 1 | 0.33 |
| Aug. Lagrangian | TR | $10^{-7}$ | $10^{-3}$ | $10^7$ | 200 | 1 | 0.06 |
| Aug. Hamiltonian | TR | $10^{-7}$ | $2 \cdot 10^{-3}$ | $10^9$ | 0.1 | 2000 | 0.13 |
| ALi3 | TR | $10^{-5}$ | $10^{-3}$ | $10^9$ | – | – | 0.07 |

Next, the simulations were repeated for a maximum admissible energy drift of 0.001 J, as required by the problem definition in [14]. With the exception of the augmented Hamiltonian formulation, it was impossible to meet this requirement using the forward Euler integrator with reasonable step-sizes. The trapezoidal rule was used as an alternative. This integrator introduces an iterative process in each time-step. It was observed that this process may diverge in the proximity of a singularity. This requires the detection of divergence and the interruption of the iteration for the simulation to proceed successfully. Results are summarized in Table 2. Similar results were obtained for a 10 s simulation of the motion of the double four-bar linkage and are shown in Table 3.

Table 3: Best performances obtained with each formulation in the 10 s simulation of the double four-bar linkage motion, for a maximum energy drift of 0.1 J. The selected integrators were the forward Euler method (FE) and the trapezoidal rule (TR).

| Formulation | Integrator | Tolerance | $h$ (s) | $\alpha$ | $\omega$ | $\xi$ | elapsed time (s) |
|---|---|---|---|---|---|---|---|
| Penalty | FE | – | $2 \cdot 10^{-5}$ | $10^7$ | 30 | 1 | 2.50 |
| Aug. Lagrangian | FE | – | $5 \cdot 10^{-6}$ | $10^7$ | 10 | 1 | 12.21 |
| Aug. Hamiltonian | FE | – | $10^{-3}$ | $10^9$ | 0.1 | 1000 | 0.07 |
| Penalty | TR | $10^{-7}$ | $5 \cdot 10^{-3}$ | $10^8$ | 25 | 1 | 0.04 |
| Aug. Lagrangian | TR | $10^{-7}$ | $5 \cdot 10^{-3}$ | $10^8$ | 20 | 1 | 0.05 |
| Aug. Hamiltonian | TR | $10^{-7}$ | $5 \cdot 10^{-3}$ | $10^9$ | 0.1 | 1000 | 0.10 |
| ALi3 | TR | $10^{-7}$ | $10^{-2}$ | $10^9$ | – | – | 0.02 |

The numerical experiments showed that a robust and efficient performance in the simulation of systems with singular configurations depends not only on the selected dynamic formulation, but also on the numerical integration formulas. For instance, the augmented Hamiltonian formulation shows very good energy conservation properties with an explicit single-step integrator like the forward Euler scheme. This allows one to carry out the simulations with a step-size larger than the one used with the penalty or augmented Lagrangian methods, as it can be seen in Tables 1 and 3. This comparative advantage is lost if the trapezoidal rule is used instead. The ALi3 algorithm with projections of velocities and accelerations showed a very robust behaviour. Possible reasons for

this are the implementation of the numerical integrator in Newton-Raphson form with the generalized coordinates as primary variables instead of fixed-point iteration, and the use of projections to remove constraint violations.

## 5 Conclusions

Penalty-based Lagrangian methods for multibody system dynamics can deal with rank-deficient Jacobian matrices but still suffer from numerical difficulties near singular configurations. These problems give rise to impact forces that can introduce sudden variations of the mechanical energy and cause the simulation to fail. In this research, benchmark problems were used to compare several augmented Lagrangian formulations in terms of their ability to carry out an efficient simulation while keeping the mechanical energy constant. It was found that the selection of the numerical integrator plays a key role in this. In particular, iterative integrators may diverge at the singularity, and so provisions must be made to stop the iteration process if this happens. In all cases, keeping the constraint violations at the configuration level under a certain threshold was required to obtain a successful simulation. This constitutes a guiding principle in the adjustment of the formulation parameters. Additionally, the formulations must be robust enough to deal with large impact forces. This suggests that implementing the algorithms in Newton-Raphson form can be advantageous in problems with singularities, which is currently an open line of research.

### Acknowledgments

The first author would like to acknowledge the support of the Spanish Ministry of Economy through its post-doctoral research program Juan de la Cierva, contract No. JCI-2012-12376.

## REFERENCES

[1] H. Goldstein. Classical Mechanics. Addison-Wesley, 1980.

[2] E. Bayo, J. García de Jalón, and M. A. Serna. A modified Lagrangian formulation for the dynamic analysis of constrained mechanical systems. Computer Methods in Applied Mechanics and Engineering, 71(2):183–195, 1988.

[3] E. Bayo, J. García de Jalón, A. Avello, and J. Cuadrado. An efficient computational method for real time multibody dynamic simulation in fully Cartesian coordinates. Computer Methods in Applied Mechanics and Engineering, 92:377–395, 1991.

[4] E. Bayo and R. Ledesma. Augmented Lagrangian and mass–orthogonal projection methods for constrained multibody dynamics. Nonlinear Dynamics, 9(1-2):113–130, 1996.

[5] J. Cuadrado, J. Cardenal, P. Morer, and E. Bayo. Intelligent simulation of multibody dynamics: Space–state and descriptor methods in sequential and parallel computing environments. Multibody System Dynamics, 4(1):55–73, 2000.

[6] D. Dopico, F. González, J. Cuadrado, and J. Kövecses. Determination of holonomic and nonholonomic constraint reactions in an index-3 augmented Lagrangian formulation with velocity and acceleration projections. Journal of Computational and Nonlinear Dynamics, 9(4):paper 041006, 2014.

[7] D. Dopico, A. Luaces, M. González, and J. Cuadrado. Dealing with multiple contacts in a human-in-the-loop application. Multibody System Dynamics, 25(2):167–183, 2011.

[8] B. Ruzzeh and J. Kövecses. A penalty formulation for dynamics analysis of redundant mechanical systems. Journal of Computational and Nonlinear Dynamics, 6(2):paper 021008, 2011.

[9] F. González, M. A. Naya, A. Luaces, and M. González. On the effect of multirate co-simulation techniques in the efficiency and accuracy of multibody system dynamics. Multibody System Dynamics, 25(4):461 – 483, 2011.

[10] E. Bayo, J. M. Jiménez, M. A. Serna, and J. M. Bastero. Penalty based Hamiltonian equations for the dynamic analysis of constrained mechanical systems. Mechanism and Machine Theory, 29(5):725 – 737, 1994.

[11] E. Bayo and A. Avello. Singularity-free augmented Lagrangian algorithms for constrained multibody dynamics. Nonlinear Dynamics, 5(2):209–231, 1994.

[12] J. Naudet, D. Lefeber, F. Daerden, and Z. Terze. Forward dynamics of open-loop multibody mechanisms using an efficient recursive algorithm based on canonical momenta. Multibody System Dynamics, 10(1):45–59, 2003.

[13] P. Malczyk, J. Frączek, and K. Chadaj. A parallel algorithm for multi-rigid body system dynamics based on the Hamilton's canonical equations. In S.-S. Kim and J. H. Choi, editors, Proceedings of the 3rd Joint International Conference on Multibody System Dynamics, Busan, Korea, 2014.

[14] IFToMM Technical Committee for Multibody Dynamics. Library of computational benchmark problems – URL: http://www.iftomm-multibody.org/benchmark, 2015.

[15] J. García de Jalón and E. Bayo. Kinematic and Dynamic Simulation of Multibody Systems. The Real–Time Challenge. Springer–Verlag, 1994.

[16] J. Baumgarte. Stabilization of constraints and integrals of motion in dynamical systems. Computer Methods in Applied Mechanics and Engineering, 1(1):1–16, 1972.

[17] N. M. Newmark. A method of computation for structural dynamics. Journal of the Engineering Mechanics Division, ASCE, 85(EM3):67–94, 1959.

[18] J. García de Jalón and M. D. Gutiérrez-López. Multibody dynamics with redundant constraints and singular mass matrix: existence, uniqueness, and determination of solutions for accelerations and constraint forces. Multibody System Dynamics, 30(3):311–341, 2013.

[19] F. González and J. Kövecses. Use of penalty formulations in dynamic simulation and analysis of redundantly constrained multibody systems. Multibody System Dynamics, 29(1):57–76, 2013.

[20] M. González, D. Dopico, U. Lugrís, and J. Cuadrado. A benchmarking system for MBS simulation software: Problem standardization and performance measurement. Multibody System Dynamics, 16(2):179–190, 2006.

[21] J. Kövecses. Dynamics of mechanical systems and the generalized free–body diagram – part I: General formulation. Journal of Applied Mechanics, 75(6):paper 061012, 2008.

[22] W. Blajer. Augmented Lagrangian formulation: Geometrical interpretation and application to systems with singularities and redundancy. Multibody System Dynamics, 8(2):141 – 159, 2002.

[23] P. Flores, M. Machado, E. Seabra, and M. Tavares da Silva. A parametric study on the Baumgarte stabilization method for forward dynamics of constrained multibody systems. Journal of Computational and Nonlinear Dynamics, 6(1):paper 011019, 2011.